

# Mammographic Breast Positioning Assessment via Deep Learning

Toygar Tanyel<sup>1</sup>, Nurper Denizoglu<sup>2</sup>, Mustafa Ege Seker<sup>3</sup>, Deniz Alis<sup>4</sup>,  
Esma Cerekci<sup>5</sup>, Ercan Karaarslan<sup>4</sup>, Erkin Aribal<sup>4</sup>, and Ilkay Oksuz<sup>6</sup>

<sup>1</sup> Istanbul Technical University, Biomedical Engineering Graduate Program

<sup>2</sup> Acibadem Healthcare Group, Department of Radiology

<sup>3</sup> Acibadem Mehmet Ali Aydinlar University, School of Medicine

<sup>4</sup> Acibadem Mehmet Ali Aydinlar University, School of Medicine, Dept. of Radiology

<sup>5</sup> Sisli Hamidiye Etfal Training and Research Hospital

<sup>6</sup> Istanbul Technical University, Department of Computer Engineering  
{tanyel23, oksuzilkay}@itu.edu.tr

**Abstract.** Breast cancer remains a leading cause of cancer-related deaths among women worldwide, with mammography screening as the most effective method for the early detection. Ensuring proper positioning in mammography is critical, as poor positioning can lead to diagnostic errors, increased patient stress, and higher costs due to recalls. Despite advancements in deep learning (DL) for breast cancer diagnostics, limited focus has been given to evaluating mammography positioning. This paper introduces a novel DL methodology to quantitatively assess mammogram positioning quality, specifically in mediolateral oblique (MLO) views using attention and coordinate convolution modules. Our method identifies key anatomical landmarks, such as the nipple and pectoralis muscle, and automatically draws a posterior nipple line (PNL), offering robust and inherently explainable alternative to well-known classification and regression-based approaches. We compare the performance of proposed methodology with various regression and classification-based models. The CoordAtt UNet model achieved the highest accuracy of  $88.63\% \pm 2.84$  and specificity of  $90.25\% \pm 4.04$ , along with a noteworthy sensitivity of  $86.04\% \pm 3.41$ . In landmark detection, the same model also recorded the lowest mean errors in key anatomical points and the smallest angular error of 2.42 degrees. Our results indicate that models incorporating attention mechanisms and CoordConv module increase the accuracy in classifying breast positioning quality and detecting anatomical landmarks. Furthermore, we make the labels and source codes available to the community to initiate an open research area for mammography, accessible at <https://github.com/tanyelai/deep-breast-positioning>.

**Keywords:** Breast cancer · Mammography · Deep learning · Positioning assessment

## 1 Introduction

Breast cancer remains the most common cancer and leading cause of cancer-related deaths among women globally [3]. Mammography screening is the most

effective method for early detection, significantly reducing mortality rates [12]. Thus, many countries have adopted national screening programs [4].

A standard mammogram includes craniocaudal (CC) and mediolateral oblique (MLO) views, with the MLO view being crucial as it captures nearly the entire breast tissue, especially the upper quadrant where cancer frequently occurs. Proper positioning in mammography is vital, as poor positioning can lead to diagnostic errors and necessitate repeat exams, increasing costs and causing stress for patients [5, 9, 11, 17]. There is a pressing need for automated systems that can instantly evaluate the quality of mammogram positioning, allowing technologists to take immediate corrective action if necessary.

Recent advancements in deep learning (DL) have shown promising results in breast cancer diagnostics, often matching or surpassing radiologists in accuracy [7, 14]. However, less focus has been given to using DL for assessing mammography positioning. This gap presents an opportunity to improve the evaluation process right after image acquisition. Traditionally, studies have relied on classification-based DL approaches involving qualitative expert assessments [2, 18] or by dividing related tasks into separate regression processes [8], which can introduce additional complexity and affect the explainability and objectivity of the results.

Our work introduces a novel deep learning methodology that quantitatively evaluates image positioning quality in MLO views. By identifying key anatomical features such as the nipple and pectoralis muscle, and automatically drawing a perpendicular posterior nipple line (PNL) to the pectoralis muscle or film edge, our methodology provides a robust and superior alternative to traditional classification-based approaches. We demonstrate the effectiveness of our method on existing models, showcasing its potential to enhance mammography positioning assessments.

## 2 Materials

In this section we provide information on the dataset and the ground truth criteria for correct MLO positioning.

### 2.1 Study Sample

We used the VinDr Mammography dataset [13], an open-access collection of 5000 exams from two hospitals in Vietnam (2018-2020). From this, we selected 1000 exams, each with two MLO view mammograms from both breasts, totaling 2000 images. Exams were split into training, validation, and testing sets with an 80%/10%/10% split, ensuring a balanced representation of clinical outcomes. According to the PNL criteria, MLO-view positioning in the datasets was classified as 967 good and 633 poor for training, 108 good and 92 poor for validation, and 123 good and 77 poor for testing.

## 2.2 Image Positioning Quality Criterion

Several international systems assess the quality of mammography images in MLO views based on criteria like the angle, width, and length of the pectoral muscle, its border angulation, and the distance between the pectoral muscle and the nipple. The primary goal is to ensure maximum breast tissue coverage. Some criteria, such as the distance from the pectoral muscle to the nipple, are subjective and impractical [16]. The angle and dimensions of the pectoral muscle lack universal standards. A consistent criterion is that the PNL, drawn from the nipple to the pectoralis muscle at a right angle, intersects the pectoralis muscle. This method is endorsed by the American College of Radiology and the Royal Australian and New Zealand College of Radiologists [1, 10, 15, 16, 19] and is adopted as our study’s reference standard.

## 2.3 Ground Truthing Process

Ground truth annotations were performed by a board-certified breast radiologist (N.D.) with over five years of experience in breast imaging. The radiologist used a specialized workstation, featuring a browser-based annotation tool (<https://matrix.md.ai>) and a 6-megapixel diagnostic monitor (Radiforce RX 660, EIZO), to annotate mammograms. All mammograms were examined in the Digital Imaging and Communications in Medicine (DICOM) format. The radiologist marked the nipple and pectoralis muscle line on MLO views.

## 3 Methods

In this section we provide details of our pre-processing operation, loss function, model architecture and experimental setup.

### 3.1 Pre-processing Steps

The pre-processing steps for mammography images are designed to prepare the data for analysis while preserving anatomical features and spatial relationships. Initially, the midpoint of the nipple bounding boxes and the endpoints of the pectoralis muscle are extracted, yielding three critical landmarks for orientation and scale adjustments. Next, the endpoints of the pectoralis muscle are standardized by extending each line to the image boundary with a 10-pixel margin to minimize variability from radiologists’ arbitrary line terminations. Significant breast regions are then isolated by removing extensive black pixel areas around the periphery and below the breast. This involves thresholding the image to create a binary version, applying morphological opening, labeling connected regions, and cropping the image to the bounding box of the largest region. Zero-padding is applied to make the images square, preventing distortion during resizing and maintaining uniformity across the dataset. Subsequently, all images are resized to  $512 \times 512$  pixels to facilitate computational efficiency and model training while preserving necessary detail.

### 3.2 Landmark-Aware Wing Loss

Landmark-Aware Wing Loss is tailored to improve the model’s accuracy in predicting landmark coordinates. It employs a piecewise function that combines the Wing Loss’s sensitivity to small errors with a linear part to moderate the response to larger errors. The Wing Loss [6] formula is given by:

$$\mathcal{L}_{Wing}(y) = \begin{cases} w \cdot \log(1 + \frac{|y|}{\epsilon}), & \text{if } |y| < w \\ |y| - C, & \text{otherwise} \end{cases} \quad (1)$$

where  $y$  represents the absolute error between the predicted and target coordinates,  $w$  is the parameter that defines the width of the non-linear region,  $\epsilon$  controls the curvature within this region, and  $C$  is a continuity constant, defined as  $C = w - w \cdot \log(1 + \frac{w}{\epsilon})$ .

Practically, the  $\mathcal{L}_{LAW}(y)$  is calculated for each coordinate of the landmarks, leading to a comprehensive loss for each landmark by summing up the mean losses of the coordinates, i.e., mean of  $x$  and  $y$ , expressed as:

$$\mathcal{L}_{LAW} = \alpha \cdot \mathcal{L}_{Wing(L1)} + \beta \cdot \mathcal{L}_{Wing(L2)} + \gamma \cdot \mathcal{L}_{Wing(L3)} \quad (2)$$

where  $\alpha$ ,  $\beta$ , and  $\gamma$  are the weights for the landmarks.

### 3.3 Model Architectures and Techniques for Landmark Detection

We used U-Net as the backbone with coordinate convolution module (CoordConv) and attention mechanisms for landmark detection (Fig. 1). CoordConv and attention refine feature maps, improving spatial information. We also used ResNeXt50 as the backbone for landmark regression, adjusting it for single-channel input and comparing its classification and regression results. This section details these components and the landmark regression process.

**CoordConv Integration** To improve spatial awareness, we replaced the initial convolutional layer with a CoordConv layer, integrating spatial coordinates into the convolution operation. CoordConv augments the input by adding normalized spatial coordinates across height (H) and width (W), improving the model’s ability to learn spatial hierarchies:

$$\mathcal{CC}(I) = \mathcal{R}(\mathcal{B}(\mathcal{C}(\mathcal{A}(I, \{x, y\})))) ,$$

where  $\mathcal{A}(I, \{x, y\})$  adds coordinate channels to input tensor  $I$ . The  $x$ -coordinates  $\{x\}$  and  $y$ -coordinates  $\{y\}$  are normalized in the range  $[0, 1]$ , calculated as:

$$x_j = \frac{j}{W-1}, \quad y_i = \frac{i}{H-1},$$

for each pixel  $(i, j)$  in the feature map. These coordinates are repeated across the batch size and stacked to form two new channels appended to  $I$ .

$\mathcal{C}$  performs convolution with these channels, and  $\mathcal{B}$  and  $\mathcal{R}$  represent batch normalization and ReLU activation.

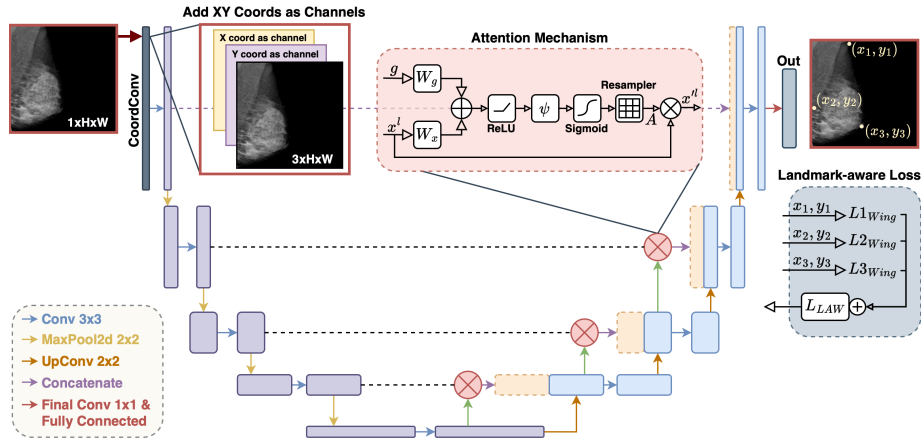


**Fig. 1.** Illustration of concepts utilized in this study as part of an ablation study. At the input layer, a single-channel grayscale mammogram is augmented to a three-channel image by introducing two additional channels that encode the X and Y spatial coordinates of each pixel. The attention mechanism refines features, and skip connections preserve spatial information. The final layer outputs landmark coordinates, optimized using landmark-aware wing loss.

**Attention Mechanism** Attention mechanisms in the U-Net model selectively focus on important features. The attention block integrates features from both encoder and decoder paths by computing attention coefficients ( $\psi$ ) using the following formulations:  $g = W_{\text{gate}} * G$  and  $x = W_x * X$ . Here,  $W_{\text{gate}}$  and  $W_x$  are convolutional filters, with  $G$  representing the gating signal from the decoder and  $X$  the feature map from the encoder. The attention coefficients  $\psi$  are computed as  $\psi = \sigma(\text{ReLU}(g + x))$ , where  $\sigma$  denotes the sigmoid activation. The attended output  $A$  is then calculated as  $A = X \cdot \psi$ . This mechanism ensures that only the most relevant features are propagated through the network to improve the precision of the output.

**ResNeXt50** We used ResNeXt50, a 50-layer deep residual network with a cardinality of 32, featuring grouped convolutions for enhanced feature learning. For landmark regression, we modified ResNeXt50 to accept single-channel input and output the required landmark coordinates. Additionally, we used the raw classification model to compare image-level classification with regression results, evaluating differences in accuracy and robustness, and demonstrating the model's versatility and effectiveness.

### 3.4 Evaluation

The evaluation checks our model's accuracy in predicting the nipple and end-points of the pectoral muscle line. We verify if the perpendicular intersection

from the nipple to the pectoral muscle (i.e., PNL) falls within the image boundaries to indicate image quality. We also measure the angular error between the original and predicted pectoral muscle lines. Additionally, we compute accuracy, sensitivity, and specificity for the model’s decisions. Euclidean distance between predicted and original landmarks in millimeters is calculated, ensuring real-world measurement accuracy. The angle error is normalized to 0-180 degrees to represent the deviation from vertical. Performance metrics are based on image quality classification, with accuracy as the proportion of correct predictions, sensitivity as the proportion of correctly identified bad quality images, and specificity as the proportion of correctly identified good quality images.

### 3.5 Experimental Setup

**Regression** We employed the R-ResNeXt50, UNet, Attention UNet, and CoordAtt UNet models, each configured with a single input channel and six output channels corresponding to the  $x, y$  coordinates of three landmarks. Training was conducted on an NVIDIA L4 GPU for 300 epochs. The Adam optimizer was used with an initial learning rate of  $1 \times 10^{-4}$ , dynamically adjusted by a CyclicLR scheduler oscillating between  $1 \times 10^{-5}$  and  $5 \times 10^{-4}$  using a triangular policy without cycle momentum. The loss function integrated Wing Loss ( $w = 3, \epsilon = 1.5$ ) and additional parameters ( $\alpha = 1.0, \beta = 1.0, \gamma = 1.0$ ) to capture both precision and geometric intricacies in landmark detection. The model with the lowest validation loss was preserved for subsequent evaluation. As an exception, the R-ResNeXt50 model was initially fine-tuned with pretrained ImageNet weights using a batch size of 8 for 150 epochs.

**Classification** For classification, we utilized a ResNeXt50 model to classify images into two positioning quality classes. Training was conducted on an NVIDIA L4 GPU with a batch size of 8 for 30 epochs, fine-tuning the model with pretrained ImageNet weights. The same optimizer and learning rate progression as in the regression setup were applied. Categorical Cross-Entropy Loss was used for loss calculations. The best-performing model, determined by a range of metrics, was preserved for subsequent evaluation.

## 4 Results

In this section, we provide results on landmark detection and binary image quality assessment.

### Models’ Performance on Landmark Detection.

Table 1 details models’ performance on landmark detection, focusing on distance errors. Direct landmark regression with ResNeXt50 (R-ResNeXt50) and vanilla UNet regression (UNet) showed higher errors for pectoral and nipple landmark detection. Attention UNet considerably improved performance both in terms of median errors, and an angular errors. CoordAtt UNet outperformed

**Table 1.** Distance errors in millimeters (mm), presented as mean ( $\mu$ ), standard deviation ( $\sigma$ ) and median ( $x \sim$ ) to mitigate the influence of challenging cases (primarily due to subjectivity of the task). Perp: Perpendicular intersection error for the line drawn from the nipple to the pectoral line. Pec1: Lower endpoint of the pectoral muscle line error. Pec2: Upper endpoint of the pectoral muscle line error. Nipple: Nipple location error. Angular: Angular difference between the predicted and original pectoral muscle line.

Models	Perp			Pec1			Pec2			Nipple			Angular		
	$\mu$	$\sigma$	$x \sim$												
R-ResNeXt50	7.13	4.23	6.49	7.33	6.01	5.24	7.93	7	6.2	4.63	1.99	4.45	2.71	2.44	1.96
UNet	9.62	7.86	8.03	8.19	6.89	6.01	14.01	14.01	10.9	6.8	5.25	5.72	3.52	3.15	2.66
Attention UNet	5.12	5.04	<b>3.56</b>	6.01	5.87	<b>4.03</b>	6.94	8.25	<b>3.95</b>	2.98	2.4	2.52	2.58	2.73	1.81
CoordAtt UNet	<b>4.99</b>	4.88	3.82	<b>5.62</b>	5.29	4.14	<b>6.49</b>	7.37	4.26	<b>2.97</b>	2.46	<b>2.45</b>	<b>2.42</b>	2.56	<b>1.75</b>

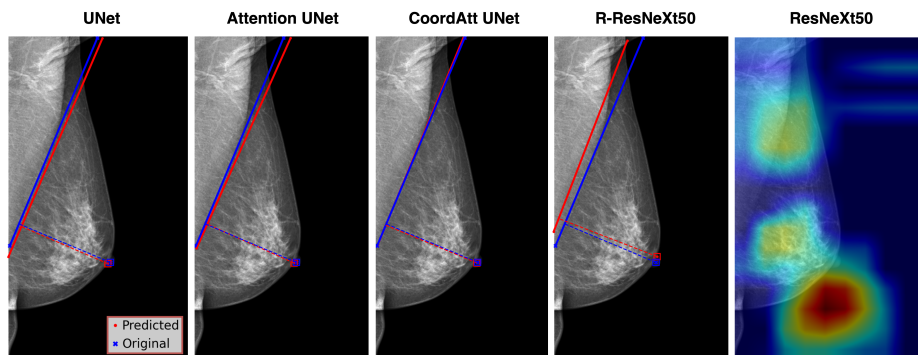


**Fig. 2.** Comparison of predicted (red) versus original (blue) landmarks in mammograms using different models: UNet, Attention UNet, CoordAtt UNet, R-ResNeXt50, and ResNeXt50. The rightmost column shows heatmaps for ResNeXt50.

others with mean errors of 4.99mm (Perp), 5.62mm (Pec1), 6.49mm (Pec2), 2.97mm (nipple), and the smallest angular error of 2.42 degrees.

#### Models' Performance on Breast Positioning Labels.

The models' performance on breast positioning labels is summarized in Table 2. The raw ResNeXt50 model used for binary classification without landmark regression achieved the lowest performance measures. Addition of landmark regression and rule-based binary classification (R-ResNeXt50), improved the performance dramatically. Vanilla UNet regression of the landmark points showed poor performance, where Attention block addition (Attention UNet) outperformed previous models. Addition of coordinate points (CoordAtt UNet) achieved comparable performance to Attention UNet showcasing superior performance in accuracy and specificity.

**Table 2.** Test results on automatically generated quality labels extracted from radiologists’ label drawings. The raw ResNeXt50 model was trained for binary classification based on image-level labels. The R-ResNeXt50 model had its last layer modified to function as a landmark regressor, predicting coordinates and overall positioning quality, similar to our proposed pipeline. Results are presented as the mean  $\pm$  standard deviation of 5 different training runs.

Model	Accuracy	Specificity	Sensitivity
ResNeXt50	73.7 $\pm$ 3.35	76.91 $\pm$ 6.26	68.57 $\pm$ 11.41
R-ResNeXt50	82.3 $\pm$ 5.03	81.42 $\pm$ 12.34	83.38 $\pm$ 10.49
UNet	70.63 $\pm$ 1.49	78.46 $\pm$ 1.56	58.12 $\pm$ 2.68
Attention UNet	88.2 $\pm$ 2.51	88.62 $\pm$ 4.11	<b>87.53 <math>\pm</math> 3.51</b>
CoordAtt UNet	<b>88.63 <math>\pm</math> 2.84</b>	<b>90.25 <math>\pm</math> 4.04</b>	86.04 $\pm$ 3.41

## 5 Discussion

In this study, we presented a novel deep learning methodology for assessing the quality of mammogram positioning, focusing on the MLO views. Our method quantitatively evaluates image positioning by identifying key anatomical features and drawing a perpendicular PNL, providing a robust alternative to traditional classification-based approaches. The evaluation of various deep learning models, including ResNeXt50, UNet, Attention UNet, and CoordAtt UNet, demonstrated considerable improvements in accuracy, specificity, and sensitivity. Notably, the CoordAtt UNet model achieved the highest performance, highlighting the effectiveness of incorporating attention mechanisms and CoordConv module (Fig. 2). This study addresses a critical unmet need in mammography screening, offering an automated, objective, and explainable solution for assessing breast positioning quality, which is crucial for accurate breast cancer diagnosis.

Despite the promising results, several limitations must be acknowledged. Our study focused exclusively on MLO views, which, while comprehensive, do not cover all diagnostic perspectives. Future work will extend the model to include CC views to provide a more holistic evaluation of mammogram positioning. Additionally, our primary criterion for evaluating positioning quality was the PNL. While robust for MLO views, the models’ effectiveness might be limited when considering other criteria, such as the angle and shape of the pectoral muscle. Future studies will aim to incorporate these additional criteria to improve the models’ versatility. The clinical impact of this research is significant, as it paves the way for more reliable and efficient mammography screening, ultimately improving early breast cancer detection and patient outcomes.

## References

1. Australian Screening Advisory Committee: National Accreditation Standards BreastScreen Australia Quality Improvement Program (Revised) (2001)

2. Brahim, M., Westerkamp, K., Hempel, L., Lehmann, R., Hempel, D., Philipp, P.: Automated assessment of breast positioning quality in screening mammography. *Cancers* **14**(19), 4704 (2022)
3. Cancer (IARC), T. I. A. for R. on Global Cancer Observatory: Global Cancer Observatory. <https://gco.iarc.fr/>, accessed on 14 May 2024
4. Duffy, S.W., Tabár, L., Chen, H.H., Holmqvist, M., Yen, M.F., Abdsalah, S., Epstein, B., Frodis, E., Ljungberg, E., Hedborg-Melander, C., et al.: The impact of organized mammography service screening on breast carcinoma mortality in seven swedish counties: a collaborative evaluation. *Cancer: Interdisciplinary International Journal of the American Cancer Society* **95**(3), 458–469 (2002)
5. Feig, S.A.: Image quality of screening mammography: effect on clinical outcome. *AJR Am J Roentgenol* **178**, 805–807 (2002)
6. Feng, Z.H., Kittler, J., Awais, M., Huber, P., Wu, X.J.: Wing loss for robust facial landmark localisation with convolutional neural networks. In: *Proceedings of the IEEE conference on computer vision and pattern recognition*. pp. 2235–2245 (2018)
7. Geras, K.J., Mann, R.M., Moy, L.: Artificial intelligence for mammography and digital breast tomosynthesis: current concepts and future perspectives. *Radiology* **293**(2), 246–259 (2019)
8. Gupta, V., Taylor, C., Bonnet, S., Prevedello, L.M., Hawley, J., White, R.D., Flores, M.G., Erdal, B.S.: Deep learning-based automatic detection of poorly positioned mammograms to minimize patient return visits for repeat imaging: A real-world application. *arXiv preprint arXiv:2009.13580* (2020)
9. Gürdemir, B., Aribal, E.: Assessment of mammography quality in Istanbul. *Diagn Interv Radiol* **18**, 468–472 (2012)
10. Hendrick, R.E., Bassett, L., Botsco, M.A., et al.: *Mammography quality control manual*. Royal American College of Radiologists (1999)
11. Mackenzie, A., Warren, L.M., Wallis, M.G., Given-Wilson, R.M., Cooke, J., Dance, D.R., Chakraborty, D.P., Halling-Brown, M.D., Looney, P.T., Young, K.C.: The relationship between cancer detection in mammography and image quality measurements. *Physica Medica* **32**(4), 568–574 (2016)
12. Magnus, M.C., Ping, M., Shen, M.M., Bourgeois, J., Magnus, J.H.: Effectiveness of mammography screening in reducing breast cancer mortality in women aged 39–49 years: a meta-analysis. *Journal of women’s health* **20**(6), 845–852 (2011)
13. Nguyen, H.T., Nguyen, H.Q., Pham, H.H., Lam, K., Le, L.T., Dao, M., Vu, V.: Vindr-mammo: A large-scale benchmark dataset for computer-aided diagnosis in full-field digital mammography. *Scientific Data* **10**(1), 277 (2023)
14. Rodriguez-Ruiz, A., Lâng, K., Gubern-Merida, A., Broeders, M., Gennaro, G., Clauser, P., Helbich, T.H., Chevalier, M., Tan, T., Mertelmeier, T., et al.: Stand-alone artificial intelligence for breast cancer detection in mammography: comparison with 101 radiologists. *JNCI: Journal of the National Cancer Institute* **111**(9), 916–922 (2019)
15. Royal Australian and New Zealand College of Radiologists: *Mammography quality assurance program* (2002)
16. Spuur, K., Hung, W.T., Poulos, A., Rickard, M.: Mammography image quality: model for predicting compliance with posterior nipple line criterion. *European journal of radiology* **80**(3), 713–718 (2011)
17. U.S. Food and Drug Administration: Positioning Responsible For Most Clinical Image Deficiencies, Failures. <https://www.fda.gov/Radiation-EmittingProducts/MammographyQualityStandardsActandProgram/FacilityScorecard/ucm495378.html> (2016), accessed on 14 May 2024

18. Watanabe, H., Hayashi, S., Kondo, Y., Matsuyama, E., Hayashi, N., Ogura, T., Shimosegawa, M.: Quality control system for mammographic breast positioning using deep learning. *Scientific Reports* **13**(1), 7066 (2023)
19. Wilson, R., Liston, J.: Quality assurance guidelines for radiographers. NHSBSP Publication, 2nd edn. (2011)